High Catalytic Activity for CO Oxidation of Gold Nanoparticles Confined in Acidic Support Al-SBA-15 at Low Temperatures

Chia-Wen Chiang,[†] Aiqin Wang,[†] Ben-Zu Wan,[‡] and Chung-Yuan Mou*,[†]

Center for Condensed Matter Sciences and Department of Chemistry and Department of Chemical Engineering, National Taiwan University, Taipei, Taiwan 106

Received: May 31, 2005; In Final Form: July 27, 2005

While there is a large number of recent studies of Au nanocatalysts supported on metal oxides, low-temperature CO oxidation under an acidic environment has not yet been accomplished. Over a novel acidic Al-SBA-15 support, uniformly distributed gold nanoparticles with sizes ~2.7 nm were obtained by a successive procedure of aminosilane grafting, gold adsorption−reduction, and then high-temperature hydrogen treatment. The catalyst system, Au@Al-SBA-15, exhibits extraordinarily high activity for CO oxidation at 80 °C. By varying the Si/Al ratio of the support, the dependence of the catalytic activity on the support Si/Al ratio was found in the CO oxidation reaction.

Introduction

Although gold is rather inert in its bulk form, highly dispersed gold nanoparticles with dimensions less than 5 nm have been shown to be active for a number of oxygen transfer reactions, especially for low-temperature CO oxidation.[1−3] The catalytic activity depends not only on the particle size of Au but also on the nature of the support and the preparation method of the catalyst.[4−6] These factors are often inter-related such that their separate contributions cannot be easily disentangled. The activity of a supported Au catalyst is governed by a complex combination of contributions of the particle morphology, metal dispersion, and electronic properties of the metal.

For the much-studied catalysis of CO oxidation, a variety of metal oxides has been studied as support for highly dispersed Au catalyst systems.[7] The nature of support affects both the activation of the oxygen and the morphology of the dispersed Au nanoparticles. Generally, oxides with either redox property (such as MnO_x) or strong basicity (such as MgO) are found to give Au nanocatalyst systems of better performance.[7] Au nanoparticles supported on an acidic support are much less explored because of difficulties in their preparation. However, they are highly desirable for the fuel cell applications, such as in PROX (preferential oxidation of CO) system, which is usually operated in a strongly acidic environment.[8] Recently, Okumura et al.[9] observed that gold nanoparticles deposited onto acidic supports such as aluminosilicates and activated carbon by gas phase grafting methods have a very low activity for CO oxidation. Highly active Au catalysts for CO oxidation on acidic supports are still unknown.

In this paper, we report a study of CO oxidation catalyzed by Au supported on acidic mesoporous silicates. There are two factors against its catalyst performance. First, due to the weak metal−support interaction, the Au nanoparticles on silica tend to be mobile and sinter during the high-temperature pretreatment of the catalyst. Second, normal aluminosilicate interacts only weakly with oxygen. A better method for the activation of oxygen on aluminosilicate has to be found.

Mesoporous aluminosilicate materials seem to be an ideal host for metallic nanoparticles due to well-defined pores and ability of surface functionalization.[10] A channel system of pore sizes in the range of 3 to 5 nm, the optimum size for catalysis, with rigid pore walls would limit the size of confined gold. Recently, we have successfully employed propylamine-functionalized MCM-41 silica (without Al) to confine Au nanoparticles.[11] However, the gold particles would still agglomerate to exceed the pore size during calcination due to the weak confinement exerted by the thin wall of MCM-41. In contrast, SBA-15 may be a better choice of support because its thicker wall can provide a stronger confinement. Moreover, we have recently developed SBA-15 mesoporous silica free-standing films with vertical channels.[12] This makes the channel length uniform in the range of ~80 nm. Thus, the short vertical channels of the SBA-15 thin film will facilitate the transport of reactant and product molecules. It is known that the acidity of molecular sieves becomes higher with more incorporation of Al. In the present paper, we used aluminum-substituted Al-SBA-15 thin films as supports to confine the gold nanoparticles and obtained a uniform size distribution of gold particles at about 3 nm. By varying the Al content in the support, an interesting Si/Al ratio effect on the CO oxidation reaction was found for the first time.

For better understanding the preparation and catalytic action of of Au confined in mesoporous aluminosilicate Al-SBA-15, various characterization techniques were employed. ^{27}Al NMR spectra were measured for the catalyst to understand its dispersion. XRD and TEM were used to measure the porosity and particle size distribution. For understanding the oxygen activation, electron paramagnetic resonance (EPR) was used to monitor the evolution of catalysis action under various pretreatment methods. It is found that a high-temperature reduction of the catalyst is crucial for good activity in the catalysis of CO oxidation.

Experimental Procedures

Preparation of the Catalyst. We report first the synthesis of the aluminosilicate Al-SBA-15 mesoporous thin film with vertical channel structures. The procedure was modified from

* Corresponding author. E-mail: cymou@ntu.edu.tw. Fax: +886-2-2366-0954.
[†] Center for Condensed Matter Sciences and Department of Chemistry.
[‡] Department of Chemical Engineering.

10.1021/jp052867v CCC: $30.25
Published on Web 08/31/2005

TABLE 1: Characterization Results for Calcined Al-SBA-15 Thin Film with Different Si/Al Ratios and Corresponding Supported Gold Catalysts

	calcined Al-SBA-15 thin film				Au@APT S-Al-SBA-15 thin film			
							Au size (nm)[f]	
Si/Al[a]	d(100) (nm)[b]	SA BET (m^2/g)	D_{pore} (nm)	V (cm^3/g)[c]	APTS loading[d] (mmol/g of SiO_2)	Au loading[e] (wt %)	as-synthesized	after H_2 reduction
58	8.62	603	4.2	0.50	2.23	19.20	1.9 ± 0.6	2.6 ± 0.6
48	8.89	647	4.9	0.56	2.66	19.83	1.8 ± 0.9	2.8 ± 0.8
39	9.03	556	4.9	0.51	2.92	17.22	1.4 ± 0.4	2.6 ± 0.6
32	10.01	634	4.6	0.54	3.03	17.97	1.6 ± 0.4	3.0 ± 0.8
29	10.39	598	4.6	0.52	3.00	16.22	1.3 ± 0.5	2.7 ± 1.0
20	10.13	535	5.2	0.53	2.05	16.44	2.1 ± 1.0	2.7 ± 0.6

[a] The Si/Al molar ratios in products are determined by ICP. [b] d(100) calculated from Bragg equation: $2d \sin\theta = n\lambda$ ($\lambda = 0.1326$ nm). [c] N_2 adsorption volume at $P/P_0 = 0.9$. [d] APTS loading detected by EA. [e] Au loading detected by ICP-AES. [f] Measured by TEM.

the method in our previous report for SBA-15 silica (without Al).[12] Then, we modified the surface with amino functionality for the loading of gold nanoparticles.

(a) To Synthesize Al-SBA-15 Thin Film. In brief, 0.7 g of pluronic P123 ($EO_{20}PO_{70}EO_{20}$) and a suitable amount of sodium aluminate were dissolved in 25 g of water, with the pH value adjusted to neutral, followed by the addition of a surfactant mixture solution including 0.75 g of cetyltrimethylammonium bromide (C_{16}TMAB) and 1.00 g of sodium dodecyl sulfate (SDS). Then, the sodium silicate solution, with the pH value adjusted to 5 to 6, was added. The reaction proceeded at 40 to 50 °C for a certain amount of time. The resulting precipitate was filtered and collected.

(b) To Prepare Surface-Modified Mesoporous Silica. To obtain high loadings of gold, the as-synthesized Al-SBA-15 thin film was first surface-functionalized by 3-aminopropyltrimethoxysilane (APTS). A direct method of surface silyl modification and simultaneous surfactant removal of mesoporous silica was employed to obtain a silane loading of about 2−3 mmol/g of SiO_2.[13] This direct method is known to lead to high and uniform surface loadings of silanes. A proper amount of Al-SBA-15 was immersed in an ethanol solution of the silane APTS and refluxed for 12−24 h at 80−90 °C. The products were recovered by filteration, washed with ethanol, and dried. The surfactants were also extracted during the same procedure.

(c) To Prepare the Au-Containing Mesoporous Silica. A gold loading of 15−20 wt % was achieved by adding 20 mL of a 25.4 mM aqueous $HAuCl_4$ solution to 1 g of functionalized Al-SBA-15 thin film. The mixture was continuously stirred for 30 min. Then, the solid was filtered and dried in ambient conditions. Reduction of Au(III) was performed by adding 10 mL of a 0.1 M $NaBH_4$ aqueous solution to 0.5 g of the composite. After filtering and drying, the as-synthesized solid (denoted as Au@APTS-Al-SBA-15) was obtained.

Catalysis Tests. Before catalysis tests, the as-synthesized (without calcinations) catalyst was pretreated by heating to 600 °C under 10% H_2/N_2 flow and holding for 1 h and then was cooled to room temperature under N_2 flow.

The catalysis test was run in a similar manner as previously reported.[11] The catalytic measurements were carried out in a packed bed within a quartz-tubular reactor (7 mm i.d.) under atmospheric pressure. A reaction gas containing 1% CO in air was passed over 20 mg of catalyst (after pretreatment) with a flow rate of 33 mL/min. The water vapor content in the reactant stream was no more than 4 ppm. The composition in the reactor out-stream was analyzed by using a Shimadzu GC-8A gas chromatography. The catalyst was denoted as Au@Al-SBA-15. This hydrogen reduction step at high temperature turns out to be crucial for good catalytic activity.

Charaterization Techniques. The powder X-ray diffraction patterns (XRD) were measured on a Scintag X1 reflection diffractometer operating with Cu Kα radiation. N_2 adsorption−desorption isotherms were performed at 77 K on a Micromeritics ASAP 2010 instrument, and the pore size distribution was calculated from the nitrogen adsorption isotherm using the Barrett−Joyner−Halenda (BJH) method. The electron microscopy images of Au nanoparticles were recorded on a JEOL JEM-2010 operated at 200 keV, and a mean size of the Au nanoparticles was estimated from the TEM images.

Nitrogen contents of the sample were analyzed with a Perkin-Elmer 2400 CHN elemental analyzer instrument, and the APTS loading contents were calculated from the nitrogen content. Al and Au contents of the sample were analyzed with a simultaneous ICP-AES allied analytical system (Perkin Elmer 3100 XL).

All ^{27}Al MAS NMR spectra were acquired on a Brüker MLS 500P NMR spectrometer at a Lamor frequency of 130.319 MHz with a sample spinning frequency of 10−12 kHz using a single pulse sequence with a $\pi/6$ pulse and recycle delay of 300 ms.

A Brüker EMX EPR spectrometer (X-band) was employed to measure the electron paramagnetic resonance (EPR) spectra of the samples. The powder sample used for the analysis was introduced in a quartz tubing of 4 mm outside diameter. The sample was sealed under vacuum. The spectrometer was equipped with a variable temperature controller, which allowed us to record spectra at low temperatures. Typical spectrometer settings were at a microwave frequency of 9.5 GHz, microwave power of 1.99 mW, and modulation amplitude of 12 G.

Results and Discussion

Table 1 lists the textural properties of the supports and the average particle size of gold confined in the supports. When the Si/Al ratios were varied, the textual properties of these Al-SBA-15 supports, including the pore size, pore volume, and BET surface area, were almost the same. It is quite striking that the sizes of the supported Au nanoparticles, despite the variation over Al content, are excellently controlled near 2.7 nm, which happens to be the optimum size for CO oxidation. The ^{27}Al NMR in Figure 1 shows that most of the Al existed in tetrahedral framework site and that they were well-dispersed. Only in the case of very high loading at Si/Al = 20 did we observe some extra framework aluminum oxide aggregations. In the ligand grafting approach, high silane loadings lead to high loadings of gold.

To identify the position and size distribution of the gold particles on the supports, high-resolution TEM (JEM-2010) investigations have been performed over these samples, and the average sizes are summarized in Table 1. Figure 2 shows the

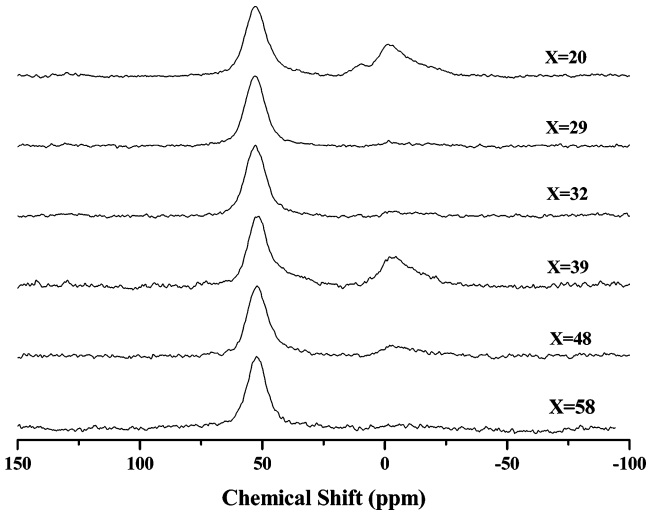

Figure 1. ^{27}Al NMR spectra of as-synthesized Al-SBA-15 thin film, Si/Al = *X*.

TEM images of all the gold-containing Al-SBA-15 samples with different Si/Al ratios. The gold particles are uniformly distributed within the channels of the SBA-15 support. The as-synthesized samples have the average particle size of Au of 1.5−2 nm (a−f in Figure 2). After reduction by H_2 at 600 °C, the Au particles became slightly larger, and the particle sizes were about 2.7 nm (g−l in Figure 2). The uniform size is highly desirable for it allows us to investigate the effect of varying the support clearly upon changing the Al content. Unlike our previous study on Au@MCM-41,[11] where the Au nanoparticles block the channels to a large extent, the gold particle in Au@Al-SBA-15 is still smaller than the pore size. The short vertical channels of the SBA-15 film are not completely blocked as one can see clearly in Figure 2. Because Al-SBA-15 has a thicker wall than MCM-41, the gold particles can be strongly confined in the channels of the support; thus, extensive sintering during the high-temperature activation process was effectively avoided.

Such uniformly distributed gold particles with an average size of 2−3 nm are expected to have a high catalytic activity for the CO oxidation reaction.[14] Figure 3a illustrates the CO conversions versus time-on-stream at 80 °C on a series of Au@Al-SBA-15 with different Si/Al ratios. The catalytic activities decay slowly over time. Although in these samples the Au nanoparticles have almost the same size, their catalytic performances varied with the Si/Al ratio. Figure 3b plots the initial CO conversion versus the Si/Al ratio. With an increase in the Si/Al ratio, the initial CO conversion increased first, attained the highest value of ca. 97% at the Si/Al ratio of 39 (determined by ICP), and then decreased with a further increase in the Si/Al ratio. In terms of the reaction rate, the catalytic activity was extraordinarily high, reaching 1.1×10^{-5} mol_{co} g_{cat}^{-1} s^{-1} for the highest point in Figure 3b. Table 2 summarizes the pretreatment conditions and the corresponding reaction rates for various catalysts of different Si/Al ratios. The reaction data were collected after 20 min reaction time. The CO oxidation reaction rates were mostly considerably higher than those reported for Au supported on Al_2O_3 and comparable to some of the best rates for Au supported on TiO_2.[3] It is worth noting that for a pure silicious SBA-15 support, Au@SBA-15 exhibited a fairly low catalytic activity (conversion ∼8% corresponding to a reaction rate of 9.0×10^{-7} mol_{co} g_{cat}^{-1} s^{-1}) at the same temperature. We also calculated the turnover frequency (TOF) based on the relationship between degree of dispersion and particle size as proposed by Bond and Thompson.[3] The results of TOF are comparable to some of the active Au catalysts reported so far.

Okumura et al.[9] observed that gold nanoparticles deposited onto acidic supports such as aluminosilicate $SiO_2-Al_2O_3$ by the gas-phase grafting method had a very low activity for CO oxidation. On the other hand, when Au was deposited on the much less acidic SiO_2, a high activity for CO could be obtained. Comparing SiO_2 and $SiO_2-Al_2O_3$, they suggested that the acidic support could not generate a high catalytic activity for low-temperature CO oxidation. In our catalyst system, we could apparently obtain a much higher activity for CO oxidation. We now would like to explore the origin of its catalytic activity.

It seems that there are at least two main factors in our Au@Al-SBA-15 system that would favor catalysis: the successful control of the particle size and the unusual pretreatment method for activating the catalyst. During the high-temperature pretreatment, the sintering of Au nanoparticles to bigger sizes would have been a serious problem. Our approach to suppress sintering by confining the gold nanocatalyst within the nanopores of SAB-15 serves to limit their sizes. In our previous work, when we both calcined and reduced Au in nanopores at high temperatures (600 °C),[11] the Au particles grew to the full limit (pore diameter) completely blocking the pore. In this work, for the mesoporous Al-SBA-15, Al on the framework not only generates acidity but also limits the particle sizes of Au. Probably, the Al sites provide defect positions of anchoring Au nanoparticles, which may be helpful for the stabilization of gold nanoparticles. Goodman and co-workers,[15,16] in a study of CO oxidation over Au/MgO catalysts, showed a direct correlation between the F-center concentration in the MgO support and the catalytic activity of the subsequently deposited Au, implying a critical role of surface defects in the anchoring and activation of Au in catalysts.

The sizes of the Au nanoparticles, at ∼2.7 nm, have the dual advantage of being smaller than the pore size and near the optimum size for catalysis. On the other hand, excessive Al may collapse the ordered mesoporous structure to some extent, giving a lower BET surface area. This may have led to some blockage of nanochannels and the observation of a decreased catalytic activity at (Si/Al) > 20.

Beside the size control of Au nanoparticles, more importantly, we believe that the activation process of the catalyst is crucial for good catalysis, especially for the inert supports such as activated carbon (AC) and aluminosilicate. It has been reported that Au nanoparticles supported on activated carbon gave a very low catalytic activity.[9] Yang et al.[17] have found that Au@SBA-15 pretreated in flowing hydrogen at 200 °C showed a relatively low reaction rate for CO oxidation (8.9×10^{-7} mol_{co} g_{cat}^{-1} s^{-1}) at 90 °C. This is more than 10 times less than the activity of our catalyst (at 80 °C). Recently, Bulushev et al.[18] found that for AC supported gold, the high-temperature reduction in H_2 (400−500 °C) was necessary to activate the catalyst.[19] We found that in our Au@Al-SBA-15 system, a harsher condition for reduction was required. The high-temperature (600 °C) pretreatment process in hydrogen was necessary for a good catalytic activity. If we only calcined, without reduction, the Au@APTS-Al-SBA-15 catalyst, the conversion for CO oxidation was nearly zero (Figure 3c). More intriguingly, if after calcination we followed with hydrogen treatment (at 600 °C), the conversion was low but nonzero (Figure 3c). Only when Au@APTS-Al-SBA-15 was directly treated with hydrogen at high temperatures did we obtain high catalytic activity as shown in Figure 3b.

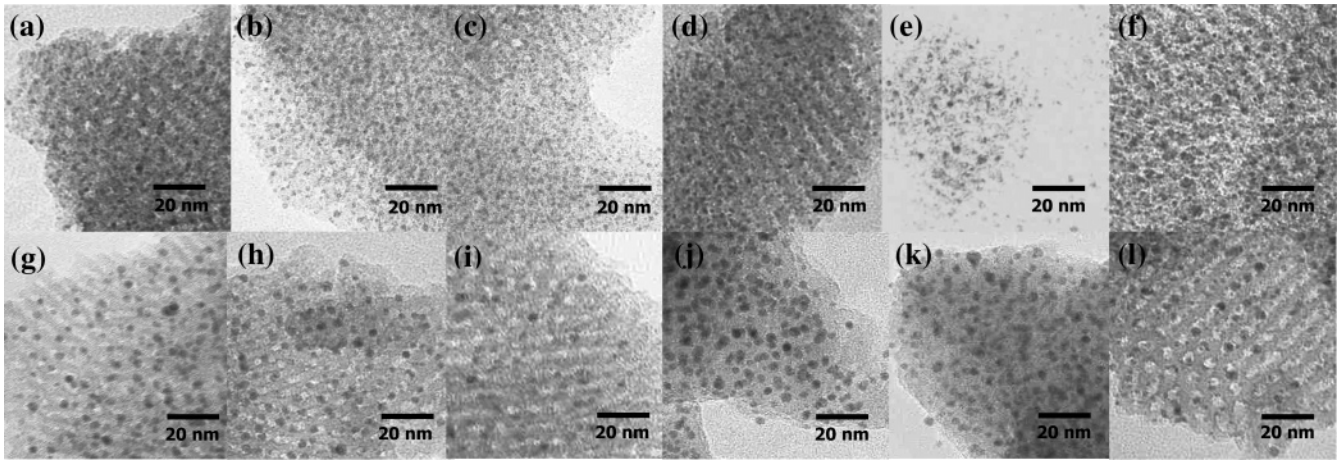

Figure 2. TEM images of as-synthesized Au@APTS-Al-SBA-15 with Si/Al ratio at (a) 58; (b) 48; (c) 39; (d) 32; (e) 29; and (f) 20. H_2-reduced sample with Si/Al ratio at (g) 58; (h) 48; (i) 39; (j) 32; (k) 29; and (l) 20.

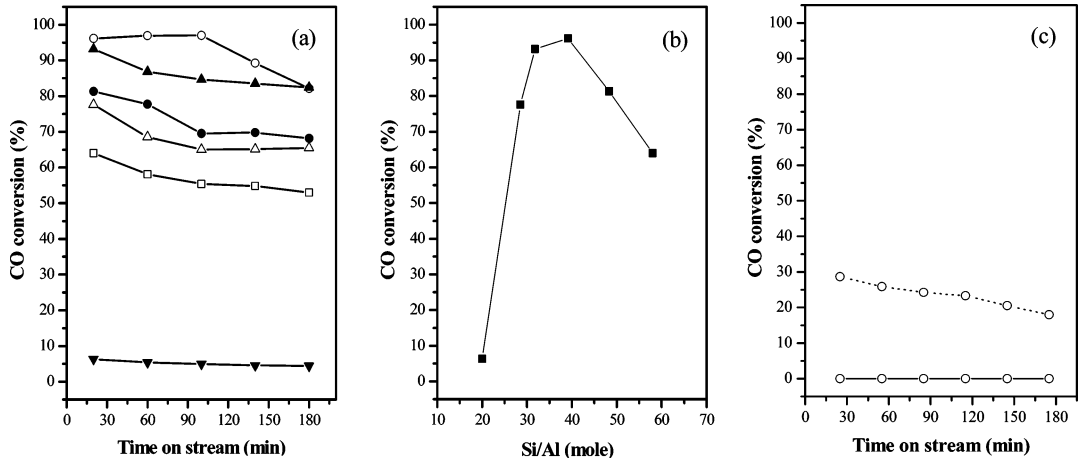

Figure 3. (a) Catalytic performance at 80 °C of Au@APTS-Al-SBA-15 catalyst with Si/Al ratios (□) 58, (●) 48, (○) 39, (▲) 32, (△) 29, and (▼) 20 after H_2-reduction. (b) Initial conversions of samples in panel a. (c) Si/Al = 39 sample after calcination (solid line) and then reduction (dot line).

TABLE 2: Pretreatment Conditions and Catalytic Performance of CO Oxidation at 80 °C for Au@APTS-Al-SBA-15

	pretreatment conditions[a]		catalytic performance		
Si/Al[b]	calcination	reduction	conversion (%)[c]	reaction rate ($mol_{co}\ g_{cat}^{-1}\ s^{-1}$)	TOF (s^{-1})[d]
58	no	yes	64	7.2×10^{-6}	1.5×10^{-2}
48	no	yes	81	9.1×10^{-6}	2.1×10^{-2}
39	no	yes	96	1.1×10^{-5}	2.5×10^{-2}
32	no	yes	93	1.0×10^{-5}	2.8×10^{-2}
29	no	yes	78	8.7×10^{-5}	2.4×10^{-2}
20	no	yes	6	7.1×10^{-7}	1.9×10^{-3}
39	yes	no	0	0	0
39	yes	yes	32	3.6×10^{-6}	8.5×10^{-3}

[a] Pretreatment was done before catalysis test. Three pretreatment conditions: reduction with N_2/H_2, calcination at 560 °C for 6 h, and calcination and then reduction. [b] The Si/Al molar ratios of the Au@APTS-Al-SBA-15 samples are determined by ICP. [c] The conversion value was taken after 20 min reaction time. [d] TOFs were calculated according to the relationship between degree of dispersion and particle size as proposed by Bond and Thompson.[3]

Intrigued by this peculiar observation, we then performed an electron paramagnetic resonance (EPR) study of the catalysts to look for the activated species superoxide O_2^- in them. EPR is a very sensitive technique for the detection of O_2^- formation on the catalyst surface. There have been many recent evidences for O_2^- in CO oxidation. A TAP (temporal analysis of products) study[18] of O_2 adsorption and the reaction of O_2 with CO, $^{20}O_2$ isotope experiments,[21] and EPR measurements[22,23] indicated that the adsorbed species O_2^- is involved in the oxidation of CO. The extra electron on the adsorbed superoxide could be a result of electron transfer from paramagnetic centers on the activated support. Okumura et al.[22] studied the interaction between CO and O_2 on Au/TiO_2 and Au/Al_2O_3 using the EPR technique. After O_2 adsorption, a signal at $g = 2.009$ was ascribed to the O_2^- radicals stabilized on the surface Ti^{4+} ions. For Au/Al_2O_3, they observed similar EPR signals at $g = 2.010$, which was ascribed to the O_2^- radicals stabilized on the Al cations.

In our EPR experiments, the catalysts were either calcined and/or prereduced in the 10% H_2/N_2 stream and then exposed to air, which resembles the pretreatment conditions used in our activity test. Figure 4 shows EPR spectra of our catalyst (at the same Si/Al = 39) at various stages of its preparation. All spectra were recorded at 77 K with a Brüker ER 200D spectrometer working in the X-band and calibrated with a DPPH standard (*g*

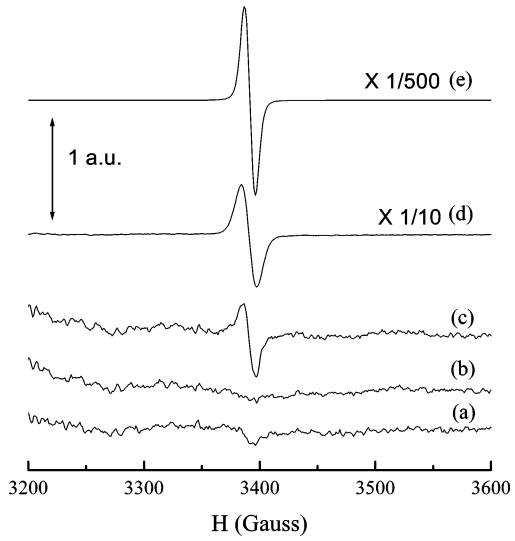

Figure 4. EPR specta of the catalyst with Si/Al = 39 at various stages of its synthesis. (a) Al-SBA-15 after calcination. (b) Au@APTS-Al-SBA-15 after calcination. (c) Al-SBA-15 after calcination and then reduction by hydrogen at 600 °C. (d) Au@APTS-Al-SBA-15 after reduction. (e) Al-SBA-15 after reduction.

= 2.0036). After various pretreatments, the catalysts were exposed to air prior to EPR measurements. Figure 4a is the EPR spectrum for the calcined (at 560 °C) mesoporous support Al-SBA-15 without Au loading. Compared to the zero signal for the as-synthesized sample (not shown here), calcination results in very weak and broad unassignable spectra. Apparently, various complicated paramagnetic defects were generated. With Au loaded (Figure 4b), the spectrum appears to be similar to Figure 4a. The corresponding catalytic activity is very low as shown in Figure 3c. The sample of Figure 4a was then subjected to high-temperature hydrogen reduction (at 600 °C), and a superoxide peak at $g = 2.009$ was generated (Figure 4c). Apparently, the hydrogen-reduced catalyst was able to transfer electrons to adsorbed oxygen to give a superoxide. This catalyst is the one giving a low but nonnegligible CO oxidation activity (Figure 3c). However, when the Au@APTS-Al-SBA-15 sample was directly reduced by hydrogen at 600 °C, it gave a much stronger signal of the superoxide O_2^- (Figure 4d). This apparently correlates well with our catalysis results (e.g., the more O_2^- is detected, the higher is the observed catalytic activity of CO oxidation). It is now known that such high-temperature reduction pretreatments would make the aluminosilicate support to generate rich defects associated with Al cations.[24] After exposure to air, the electrons trapped at such defects transfer to the adsorbed O_2 to form the superoxide O_2^-. Therefore, the EPR signals we have observed on the support probably originate from the O_2^- molecules stabilized on Al. Direct hydrogen treatment seems to remove organics and be most efficient in producing defects for superoxide adsorption. Such harsh treatment with hydrogen may have abstracted some oxygen from the Al-SBA-15 support to give electron-rich oxygen vacancies that then produce O_2^- upon oxygen adsorption.

Finally, we examined the aluminosilicate support (Al-SBA-15) without loading gold after the same hydrogen treatment. To our surprise, Figure 4e gives a much stronger signal of O_2^-. Apparently, the generation of the superoxide is not related to the gold loading. Instead, it seems to be much helped by the presence of aluminum. On the other hand, the loading of the Au nanoparticle quenches the strength of the superoxide detected. It is also well-known that Au nanoparticles quench the fluorescence of nearby fluorophores by electron transfer. However, further studies are necessary for clarifying the origin of the excellent catalytic activities reported here. For this hydrogen treated APTS-Al-SBA-15 sample, we also tested activity for CO oxidation and there is none. This is understandable because there is no gold loaded.

Conclusions

In summary, with the mesoporous Al-SBA-15 thin film as a confining support, we have obtained uniformly size-distributed gold nanoparticles within the nanochannels of Al-SBA-15. High catalytic activities for low-temperature oxidation of CO were obtained. We were able to control the size of gold nanoparticles close to 2.7 nm, which is known to be the optimum size for catalysis by gold. The small size of Au probably promotes stronger adsorption of reactants and better activation.[25] Moreover, a remarkable dependence of catalytic activity on the Si/Al ratio of the support was found. A special high-temperature treatment in hydrogen was found to be necessary for obtaining the highly active Au catalyst on the acidic support Al-SBA-15. EPR studies on the superoxide generated on Au@Al-SBA-15 indicate that the origin of catalytic activity in CO oxidation lies in the activation of oxygen on the support, while Au nanoparticles adsorb and activate the CO molecule. To our knowledge, this is the first report on the high catalytic activity of gold nanoparticles on an acidic support. Such a catalyst on an acidic support may be useful for CO removal in the PROX system.[26] Also, it may be extended to other oxidation or hydrogenation reactions.[27]

Acknowledgment. This work was supported by the Ministry of Education of Taiwan. We thank Profs. Hong-Ping Lin and Tien-Sung Lin for discussions and Mr. Shuu-Ru Liu and Chin-Kuei Kuo for help in TEM measurements.

References and Notes

(1) Haruta, M. *Catal. Today* **1997**, *36*, 153.
(2) Costello, C. K.; Yang, J. H.; Law, H. Y.; Wang, Y.; Lin, J. N.; Marks, L. D.; Kung, M. C.; Kung, H. H. *Appl. Catal. A* **2003**, *243*, 15.
(3) Bond, G. C.; Thompson, D. T. *Catal. Rev.—Sci. Eng.* **1999**, *41*, 319.
(4) Boccuzzi, F.; Chiorino, A.; Manzoli, M.; Lu, P.; Akita, T.; Ichikawa, S.; Haruta, M. *J. Catal.* **2001**, *202*, 256.
(5) Wolf, A.; Schüth, F. *Appl. Catal. A* **2002**, *226*, 1.
(6) Schubert, M. M.; Hackenberg, S.; van Veen, A. C.; Muhler, M.; Plzak, V.; Behm, R. J. *J. Catal.* **2001**, *197*, 113.
(7) Grisel, R. J. H.; Nieuwenhuys, B. E. *J. Catal.* **2001**, *199*, 48.
(8) Cameron, D.; Holliday, R.; Thompson, D. *J. Power Sources* **2003**, *118*, 29.
(9) Okumura, M.; Tsubota, S.; Haruta, M. *J. Mol. Catal. A* **2003**, *199*, 73.
(10) (a) Ghosh, A.; Patra, C. R.; Mukherjee, P.; Sastry, M.; Kumar, R. *Microporous Mesoporous Mater.* **2003**, *58*, 201. (b) Guari, Y.; Thieuleux, C.; Mehdi, A.; Reyé, C.; Corriu, R. J. P.; Gomez-Gallardo, S.; Philippot, K.; Chaudret, B.; Dutartre, R. *Chem. Commun.* **2001**, *15*, 1374.
(11) Chi, Y. S.; Lin, H. P.; Mou, C. Y. *Appl. Catal., A* **2005**, *284*, 199.
(12) Chen, B. C.; Lin, H. P.; Chao, M. C.; Mou, C. Y.; Tang, C. Y. *Adv. Mater.* **2004**, *18*, 1687.
(13) Liu, Y. H.; Lin, H. P.; Mou, C. Y. *Langmuir* **2004**, *20*, 3231.
(14) (a) Valden, M.; Lai, X.; Goodman, D. W. *Science* **1998**, *281*, 1647. (b) Haruta, M. *Catal. Today* **1997**, *36*, 153.
(15) Goodman, D. W. *Catal. Lett.* **2005**, *99*, 1.
(16) Yan, Z.; Chinta, S.; Mohamed, A. A.; Fackler, J. P., Jr.; Goodman, D. W. *J. Am. Chem. Soc.* **2005**, *127*, 1604.
(17) Yang, C. M.; Kalwei, M.; Schüth, F.; Chao, K. J. *Appl. Catal., A* **2003**, *254*, 289.
(18) Bulushev, D. A.; Yuranov, I.; Suvorova, E. I.; Buffat, P. A.; Kiwi-Minsker, L. *J. Catal.* **2004**, *224*, 8.
(19) Zhang, Z.; Jin, Z. S.; Zhang, J. W.; Zhang, Z. J.; Dang, H. X. *J. Mol. Catal. A* **2005**, *225*, 59.
(20) Olea, M.; Kunitake, M.; Shido, T.; Iwasawa, Y. *Phys. Chem. Chem. Phys.* **2001**, *3*, 627.

(21) Schubert, M. M.; Hackenberg, S.; van Veen, A. C.; Muhler, M.; Plzak, V.; Behm, R. J. *J. Catal.* **2001**, *197*, 113.
(22) Okumura, M.; Coronado, J. M.; Soria, J.; Haruta, M.; Conesa, J. C. *J. Catal.* **2001**, *203*, 168.
(23) Claus, P.; Brückner, A.; Mohr, C.; Hofmeister *J. Am. Chem. Soc*. **2000**, *122*, 11430.
(24) Lin, H. P.; Mou, C. Y. *J. Phys. Chem. B* **2000**, *104*, 8967.
(25) Rodriguez, J. A.; Pérez, M.; Jirsak, T.; Evans, J.; Hrbek, J.; González, L. *Chem. Phys. Lett.* **2003**, *378*, 526.
(26) Haruta, M. *Gold Bull.* **2004**, *37*, 27.
(27) Schimpf, S.; Lucas, M.; Mohr, C.; Rodemerck, U.; Brückner, A.; Radnik, J.; Hofmeister, H.; Claus, P. *Catal. Today* **2002**, *72*, 63.